Leaking method approach to surface transport in the Mediterranean Sea from a numerical ocean model

Judit Schneider [a,1] Vicente Fernández [b,2]
and Emilio Hernández-García [b,3]

[a]*University Potsdam, Institute for Nonlinear Dynamics, Potsdam, Germany*

[b]*Instituto Mediterráneo de Estudios Avanzados IMEDEA (CSIC-UIB) , Campus de la Universitat de les Illes Balears, E-07122 Palma de Mallorca, Spain.* [4]

Abstract

We use Lagrangian diagnostics (the *leaking* and the *exchange* methods) to characterize surface transport out of and between selected regions in the Western Mediterranean. Velocity fields are obtained from a numerical model. Residence times of water of Atlantic origin in the Algerian subbasin, with a strong seasonal dependence, are calculated. Exchange rates between these waters and the ones occupying the northern basin are also evaluated. At surface, northward transport is dominant, and involves filamental features and eddy structures that can be identified with the Algerian eddies. The impact on these results of the presence of small scale turbulent motions is evaluated by adding Lagrangian diffusion.

Key words:
Mediterranean Sea, Lagrangian transport, dynamical structures, exchange rates, ocean modelling

1 Introduction

Ocean currents transport water in such a way that parcels initially close become distant after some time (*dispersion*). Eventually water masses of different origins are put into contact, allowing them to interchange their contents

---

[1] `jotes@agnld.uni-potsdam.de`

[2] `v.fernandez@uib.es`

[3] Corresponding author: `emilio@imedea.uib.es`

[4] `http://www.imedea.uib.es/`

of heat, chemicals or nutrients (*mixing*). These two processes, dispersion and mixing, have a profound impact on the physical, chemical and biological dynamics of the ocean. The rapid development of Lagrangian techniques (Mariano et al., 2002) is enhancing our understanding of them. For example, drifter experiments, that directly track the motion of the water parcel on which the drifter has been deployed, reveal irregular trajectories and strong dependence of them on the precise position and timing of the release. The influence of coherent structures on the trajectories, such as trapping by eddies, is also observed. A common way to organize drifter data is by means of 'spaghetti plots', in which all measured trajectories are plotted together. The direction of the main currents, the presence of eddies, or the strength of tracer dispersion are easily inferred from them.

The spatial resolution of standard drifter experiments is limited by the (rather small) number of drifters that can be deployed. Increasing resolution and at the same time acquiring a truly synoptic view of Lagrangian transport requires a huge number of tracers. At present, this kind of study is only accessible for the flows produced by numerical models. A methodological problem arises now, since a 'spaghetti plot' made of the trajectories of, say, 10^5 tracers would be completely featureless and of no use. Systematic methods to select subsets of relevant trajectories and/or relevant features from them are thus needed. One of the frameworks that is being used in this context and in the general goal of understanding transport in hydrodynamical flows comes from the mathematical study of dynamical systems (Wiggins, 1992). This approach identifies the main dynamical structures that provide the skeleton organizing the full set of particle trajectories. Irregular trajectories and sensitive dependence on initial conditions are interpreted as the direct manifestation of the chaotic nature of fluid trajectories in the ocean. Coherent structures such as eddies and fronts are also linked to well studied objects in the dynamical systems approach.

Although techniques for the identification of dynamical structures in time-periodic velocity flows are well established since long time ago (Ottino, 1989; Wiggins, 1992), the consideration of aperiodic flows, as occurring in the turbulent ocean, is much more recent. A variety of methods are being tested on more or less idealized dynamical systems (Haller and Poje, 1998; Coulliette and Wiggins, 2001) and some of them applied to realistic geophysical settings (Lacorata et al., 2001; Kuznetsov et al., 2002; Joseph and Legras, 2002; d'Ovidio et al., 2004). A particularly simple methodology was proposed in Schneider et al. (2002) and applied to idealized geophysical flows (Schneider et al., 2003). The so-called *leaking method* consists in identifying the initial positions of particles that leave a given spatial region within a long enough interval of time. Alternatively, starting positions of trajectories which remain in a given region can also be identified. In both cases, the geometrical structures of these sets of positions are related to objects of dynamical relevance. In the context of chaotic dynamical systems, they are shown to have a frac-

tal structure, i.e. fine details with self-similar properties at arbitrarily small scales. The meaning of this in the ocean context is that these sets will show a fine filamentary structure which resembles satellite observations of sea surface temperature or ocean color images. From a practical point of view, the fine structure is the responsible for the different fate of trajectories starting in close and apparently equivalent positions. The structures revealed by the leaking method allow the identification of the *transport routes* between ocean regions, as well as the *barriers to transport*. The method was originally developed to display the geometry of the transport structures. But it also gives readily the relevant time scales for escape from selected regions or residence times, an information of evident oceanographic interest (Buffoni et al., 1997).

In the present paper, we apply the leaking method to a surface velocity field of the Mediterranean Sea obtained from a primitive equation ocean model under climatological atmospheric forcing. We focus in the Western Mediterranean, and characterize surface water exchange between a northern and a southern subbasin, which are areas occupied by water masses of different characteristics.

The Paper is organized as follows: In Sect. 2 we summarize the essential details of the Mediterranean Sea oceanography needed for the rest of the Paper, and we define the regions analyzed. Sect. 3 introduces the numerical model and Sect. 4 describes the methodology used, i.e. the *leaking* and the related *exchange* methods. Residence times and Lagrangian structures for leaking out of the southern part of the Western Mediterranean are presented in 5.1, and rates of north-south exchange and associated structures in 5.2. In Subsection 5.3 we explore what modifications of the above results would be induced by unresolved small-scale turbulence, modelled here as a Lagrangian diffusion process. The final Section contains our conclusions.

2 Mediterranean Sea background

The Mediterranean is a mid-latitude semi-enclosed sea connected with the Atlantic Ocean via the Strait of Gibraltar. It is composed of two principal basins, the western and the eastern basins which are connected by the Channel of Sicily. The main oceanographic characteristic of the Mediterranean Sea as a whole is that it is an evaporative basin (evaporation exceeds precipitation), and the deficit of water is supplied by the inflow of Atlantic waters from the Strait of Gibraltar. This is considered to be the main forcing mechanism of the Mediterranean circulation. In a schematic view of the surface circulation (Millot, 1987, 1999), Atlantic waters coming from the Strait of Gibraltar flow eastward along the North African coast, forming the so called Algerian current. When this current reaches the Channel of Sicily, it bifurcates. One branch follows a cyclonic (anticlockwise) path around the Western Mediterranean

3

Basin, while the other branch crosses the Channel of Sicily into the eastern basin where it also follows a general cyclonic path. The longer the water stays in the Mediterranean, the saltier it becomes due to mixing with adjacent water masses and to evaporation.

The Eastern and Western Mediterranean basins themselves can be divided in several subbasins, which are separated by topographic features (straits or channels) and clearly characterized by different water masses, patterns of circulation and characteristic forcing mechanisms (e.g heat fluxes, wind stress, rivers discharge, etc). Indeed, each of the subbasins present a variability dependent on the local forcing variability and on its own dynamics. This fact makes the Mediterranean surface circulation to be depicted as different interacting scales, including large scale, subbasin and mesoscale. The interaction between subbasin circulation and the general circulation, and the connections and water transports between subbasins, is still an open field of research of the oceanography in the Mediterranean Sea (Astraldi et al., 1999).

We concentrate in this Paper in the western basin, and characterize surface transport processes involving the relatively fresh water of Atlantic origin that fills the southern part of the basin: its residence time and its interchanges with the saltier water in the north. There is observational evidence of an intense interchange of surface waters between these two regions, in which northern saltier waters are transported to the south to close the cyclonic western Mediterranean circulation, but also southern fresher waters are found in the north (Taupier-Letage and Millot, 1988; Pinot et al., 2002; Pascual et al., 2002). These authors also suggest that the norther intrusion of southern waters is mainly due to mesoscale Algerian eddies that carry Atlantic waters from the Algerian subbasin to the Balearic Islands latitude and further north.

Fig. 1 displays the Western Mediterranean. The two rectangular boxes are associated to the north and south regions containing mainly the two different water masses. The southern box extends from 36N to 39N, and the northern one from 39N to 44.5N. The longitudinal extent of both is from 0 to 9E. The location of these geographical boundaries is arbitrary to some extent, but we have selected the boundary between the two regions to be at the same latitude as the Ibiza channel (the pass between Ibiza, the most occidental island of the Balearic Islands, and the Spanish coast) where it is known than an intense water exchange occurs (Pinot et al., 2002).

3   Mediterranean Sea numerical model

In this study, we have used the DieCAST (*Dietrich for Center Air Sea Technology*) numerical ocean model applied to the Mediterranean Sea with realistic
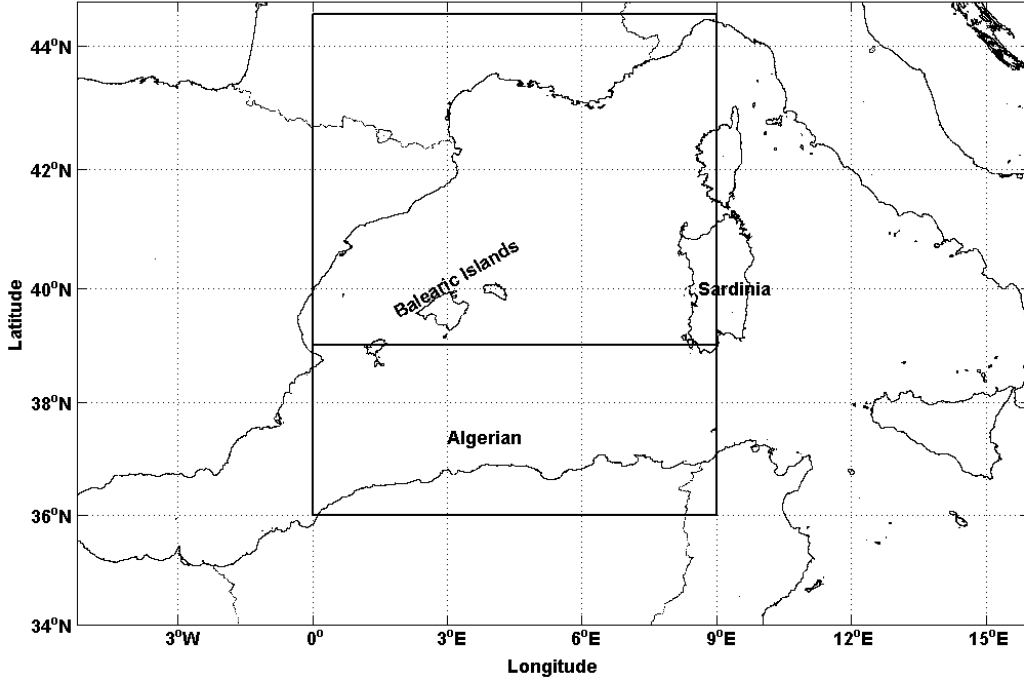
Fig. 1. The Western Mediterranean. The two rectangular boxes are the regions among which transport will be addressed. The southern box (Algerian subbasin) contains relatively fresh water of Atlantic origin, and the northern one Mediterranean saltier waters.

coastlines and topography. DieCAST (Dietrich, 1997) is a primitive equation, z-level, finite difference ocean model using the hydrostatic, incompressible and rigid lid approximations.

We summarize here some of the main properties of the model setup (see Fernández et al. (2004) for more details). The horizontal resolution is 1/8 degrees while the vertical direction is discretized in 30 levels. Horizontal eddy viscosity and diffusivity are specified to have constant values of $A_h = K_h = 10 \ m^2s^{-1}$, and are represented by a Laplacian operator. The use of these rather small values of dissipation in DieCAST is possible by the use of fully fourth-order-accurate numerics with special care to reduce numerical dispersion (Dietrich, 1997). It is noticeable that these values coincide with the value of the eddy diffusivity estimated by Okubo (1971) from measurement of tracer dispersion at several scales. Okubo results can be summarized in his empirical formula for the diffusivity (in m^2s^{-1}) as a function of spatial scale l (in m): $K_h = 2.055 \times 10^{-4} \ l^{1.15}$. This gives $10 m^2s^{-1}$ for our horizontal grid resolution ($l = \Delta x \approx 12 \times 10^3 m$ is the approximate spacing corresponding to 1/8 of degree at Mediterranean latitudes). Vertical viscosity and diffusivity are based on Pacanowski and Philander (1981), with background vertical viscosity and diffusivity set at near-molecular values (0.01 and 0.002 cm^2s^{-1}, respectively). Tracer and momentum time step is 15 minutes.

5

In order to focus on the transport mechanisms intrinsic to the internal dynamics of the Mediterranean, we excluded interannual and high-frequency fluctuation in the model atmospheric forcing. We force the model with a monthly climatological wind stress and with heat and freshwater fluxes at the sea surface constructed in such a way that the mean annual cycle of surface temperature and salinity follow the observed climatological annual cycle (Dietrich et al., 2004). In this climatological configuration, the model has been able to reproduce the correct general circulation of the basin and the major circulation features (see Fernández et al. (2004)). We stress however that since the forcing lacks any high component frequency (as the ones arising in real ocean from wind burst, storms, etc.), model output does not contain much energy at high frequencies. In particular, the intensity of the inertial oscillation period of around $17h$ is very weak. Thus it is enough to store model outputs as instantaneous values each model day. We used for this study the instantaneous model Eulerian velocity data from the second model level (representing the velocity field of a layer of 11.6 m of thickness, centered at a depth of 16 m). Using the second layer avoids the rather direct wind influence suffered by the first one. The data correspond to four years (18 to 21) of a simulation taken after the model has reached an equilibrium state for the surface circulation.

We consider just the horizontal components of the surface velocity. We acknowledge that the surface model velocity is not exactly divergenceless and, at sufficiently long times, true fluid particles will finally leave the considered layer in the vertical direction. However, vertical velocities are about three of four orders of magnitude smaller than horizontal ones and, as a consequence, model vertical mass fluxes in the situations considered here turn out to be at least one order of magnitude smaller than the horizontal mass transport. As a representative example, the vertical outflow leaving the Algerian box (see Fig. 1) is less than 4% compared with the outflow through its lateral boundaries. Moreover, Lagrangian motion in the horizontal is the adequate framework to compare with standard in-situ surface drifters, which move on a two-dimensional plane at a fixed depth. In our case, horizontal tracers can be related with surface drifters at 16 m. Therefore, we do not consider in this work vertical velocities, so that the transport properties established here should be considered mainly (as surface drifter experiments) as a tool to explore the transport processes limited to the surface layer.

4 Lagrangian diagnostics - The leaking method

The leaking method (Schneider et al., 2003, 2002), originally developed to visualize Lagrangian structures in complex flows, focus on a finite preselected region out of the full region accessible to the flow. One introduces at an initial moment t_0 a large number of fluid particles in this region and lets them

to be transported by the flow for a time span τ, definitely longer than the natural time scale of the flow. The particles are only followed until they exit the selected region. Thus, the initial ($t = t_0$) positions of these trajectories define the location of long lifetimes inside the region. It turns out that these initial positions either align in filamental features that can be shown to identify contracting directions in the flow (Ott and Tél, 1993), or they delineate coherent structures such as eddies. The reason for that lies on the existence, in typical open chaotic flows, of a very small subset of initial conditions (called the *chaotic saddle*) that never leave the selected region(Ott and Tél, 1993). The initial conditions with long lifetimes, identified with the leaking method, are the start points of trajectories attracted by the chaotic saddle and passing close enough to it. They form its so called *stable manifold* (Ott and Tél, 1993). As in the case of simpler flows approaching stagnation points, fluid elements contract in the direction of approach to the saddle, unless they are already in coherent structures such as eddies that can remain inside the study region without net stretching nor contraction. In the same way, the final ($t = t_0 + \tau$) positions of the same trajectories fall also either on coherent structures or on filaments along which trajectories are about to escape the preselected region. The tangents of this *unstable manifold* (Ott and Tél, 1993) correspond to the local stretching directions, since tracers are being stretched from the saddle along them. The shape and location of the obtained structures are functions of time (t_0 for the stable and t_f for the unstable manifold) as long as the flow is time-dependent.

The resolution with which the filamental structures are obtained depends on the length of simulated time τ (simulating for too short times, not all particles will be aligned along the contracting/stretching directions, whereas when simulating for a too long time the fine filamental structures fade out and disappear because of the decreasing number of particles that trace them) and on the initial number of tracers used (from more particles finer features can be recovered, but denser structures may become saturated). We empirically find that adequate contrast in the structures is found by deploying of the order of 10^5 particles on the boxes of Fig. 1. This means that in average (we choose the initial locations at random) the initial distance between tracers is of the order of 1-2 km.

In the cases in which the transported particles undergo standard chaotic motion, the number of fluid particles $N(t)$ that have not yet exit the region after a time $t \in (t_0, t_f)$ decays exponentially $N(t) \approx N(t_0) \, e^{-\kappa(t-t_0)}$ (Ott and Tél, 1993; Jung et al., 1993), from which a escape rate κ can be measured. Its inverse has the meaning of a *residence time* in the region. In the presence of coherent structures, however, this exponential decay slows down into a power-law at long times. Although we are restricting to horizontal motion in this Paper, we mention that the leaking method can be applied also to more complex threedimensional situations (Tuval et al., 2004).

In addition to the original leaking method, we propose here a modified version of it (that we can call the *exchange* method) in order to get additional information about exchange rates and transport structures between two subbasins: we want to consider two different regions (the northern and southern boxes in the Western Mediterranean map of Fig. 1) and calculate the transport properties between them. One of the two regions will be filled up randomly with particles. Then, the motion of the particles is calculated. In contrast to the original leaking method, particles are free to leave their starting region and to move in the whole Mediterranean. But at the moment in which they (eventually) enter the second region, the simulation of their motion is stopped. These particles are then counted as *exchanged* ones. Again, the local tangents to the initial and final distributions of non-exchanged particles identify contracting and stretching directions, and coherent structures (and the same applies to the distribution of exchanged ones) . In addition, the initial positions of the exchanged particles identify the *exchange set*, i.e., the initial locations that contribute to transport to the second area within the considered time span. Time scales for transport among the regions can be conveniently defined (see Sect. 5.2).

Motion of particles is calculated by using the Eulerian velocity fields, previously stored from the numerical simulation. Linear interpolation in time is used to downsize the 1 day interval between stored data to the 0.5 hour time-step of the 4-order Runge-Kutta used in the trajectory calculation. In space, we use bilinear interpolation to compute velocities in between the model gridpoints.

5 Results

5.1 Exit process and residence times in the southern Western Mediterranean

We apply the leaking method to the southern box depicted in Fig. 1 (comprised between 0 and 9E and between 36N and 39N). This box is traversed by the Algerian current, flowing eastwards, and contains mainly low-salinity water masses of Atlantic origin (S < 37.5 psu). We estimate the residence times inside the box, and the geometrical paths of escape.

We put at random initial positions a large number of particles in the box. Their initial positions are randomly drawn from an uniform distribution. We then follow numerically during $\tau = 90$ days the trajectories of the $N(t_0) = 122352$ particles that were not started in land. Particles are marked as escaped when they first leave the box, and their trajectories are no longer followed. The final positions of particles which remain in the box until the end of the simulation depict the unstable manifold (coherent structures and stretching
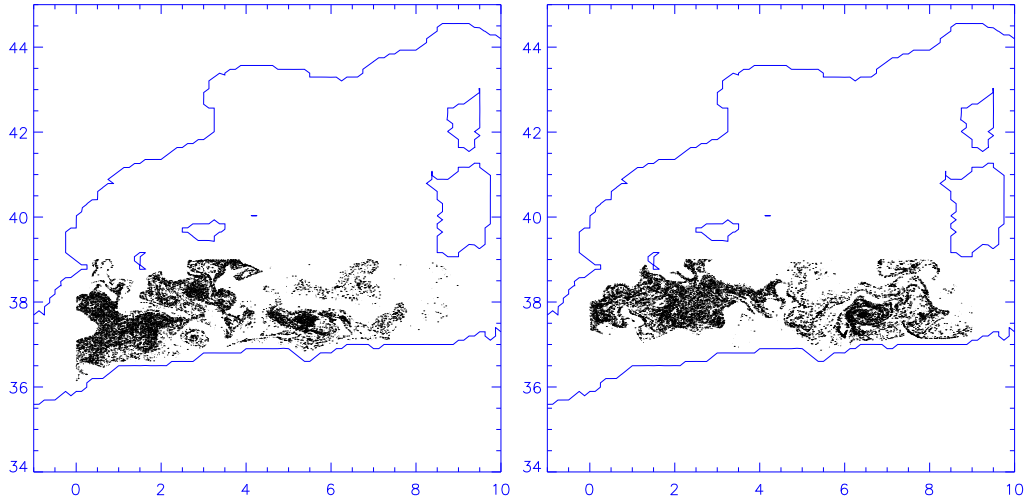
Fig. 2. Left: The initial positions of particles which did not leave the southern box during an interval of time $(t_0, t_0 + \tau)$, with the starting time t_0 at the beginning of Winter of the first simulation year and $\tau = 90$ days. They trace the stable manifold of the saddle, so that they either reveal coherent structures or align along contracting directions. Right: Final positions of the above particles, tracing out the unstable manifold and revealing additional coherent structures or stretching directions.

directions), whereas their initial positions are associated to the stable manifold (coherent structures and contracting directions). Fig. 2 shows an example of such structures, obtained by starting the Lagrangian integrations at a time t_0 corresponding to the first day of Winter (in this paper, Winter will denote the months of January, February and March, i. e. the first 90 days of the year, Spring the next three months, Summer the following ones, until Autumn which will comprise October, November and December).

We see complex geometrical structures with filamental features and also the presence of eddies. The initial location of non-escaped particles is far from compact and is interleaved with the initial location of the escaped ones, so that small displacements in this initial position will change the fate of the particle. We see that escape is more frequent when starting in the eastern part of the box, whereas particles started in the west have more chances to become trapped in structures suggestive of Algerian eddies.

The fine structure of the geometry of the escaping and non-escaping sets is better appreciated in Fig. 3. It can be though qualitatively as a blow up of Fig. 2, although, for clarity, it has been produced in a different way: a number of particles has been integrated for $\tau = 30$ days, but considering the leaking from the smaller region shown in Fig. 3. Although different in detail, the main features should be similar to the ones in Fig. 2. Filaments, eddies, and the entanglement between escaping and non-escaping positions, are particularly clear here. Of course, since some of these structures are smaller than the model
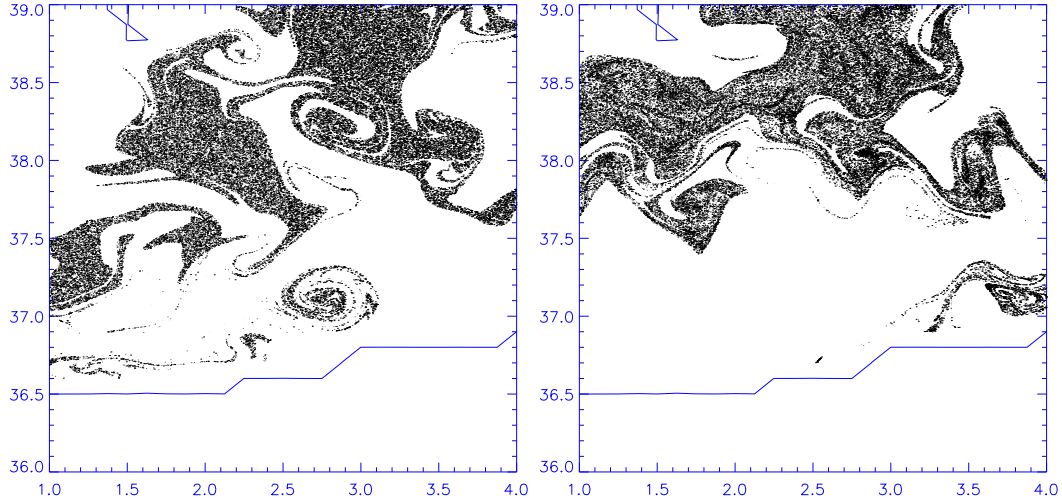
Fig. 3. Idem as Fig. 2, but using a smaller box in the leaking approach, and an integration time of $\tau = 30$ days. Qualitatively, it can be considered as a blow-up of Fig. 2.

grid size, their precise details would be dependent on any small scale processes not explicitly resolved by the model (see Sect. 5.3 for examples of this). But the existence of fine and interwoven domains of initial conditions leading to a different fate for the particles is a general feature of any flow with chaotic trajectories.

The escape rate from the original [0,9E]×[36N,39N] box can be calculated from the decay of $N(t)$, the number of non-escaped particles after a time t. For the same example of launching the particles in Winter, as before, Fig. 4 displays a clear exponential decay during the integration time, so that a escape or leaking rate ($1.93 \cdot 10^{-2}$ $days^{-1}$ for the Winter example of the figures) can be obtained from an exponential fitting. The inverse of the rate can be interpreted as a residence time inside the region (51.8 days for the example before). Table 1 shows the seasonal dependence of the rates, with the faster escape in Autumn and the slower in Summer. The yearly averaged residence time in the southern basin is 59.4 days. This residence time is comparable to estimations based on Lagrangian data, which gives a few months on average for a particle to escape from the Algerian subbasin (Millot, 1991; Salas et al., 2002).

Seasonal cycle is the main component of variability in the leaking rates (the model is forced by a seasonal atmospheric cycle), but note also the existence of a signal of interannual variability, which reflects non-forced interannual changes in ocean surface mesoscale structures due to the non-linear character of the ocean dynamics.

10

Season	leaking rates (days^{-1})	(std (days^{-1}))
Winter	$1.93 \cdot 10^{-2}$	$(1.69 \cdot 10^{-3})$
Spring	$1.38 \cdot 10^{-2}$	$(1.55 \cdot 10^{-3})$
Summer	$1.39 \cdot 10^{-2}$	$(2.35 \cdot 10^{-3})$
Autumn	$2.02 \cdot 10^{-2}$	$(1.54 \cdot 10^{-3})$
Yearly Average	$1.68 \cdot 10^{-2}$	$(3.40 \cdot 10^{-3})$

Table 1

Leaking rates out of the southern box for each season, averaged over 4 years, and the yearly average, with the corresponding standard deviation (std) characterizing the dispersion among the four years. Rates are in $1/day$.
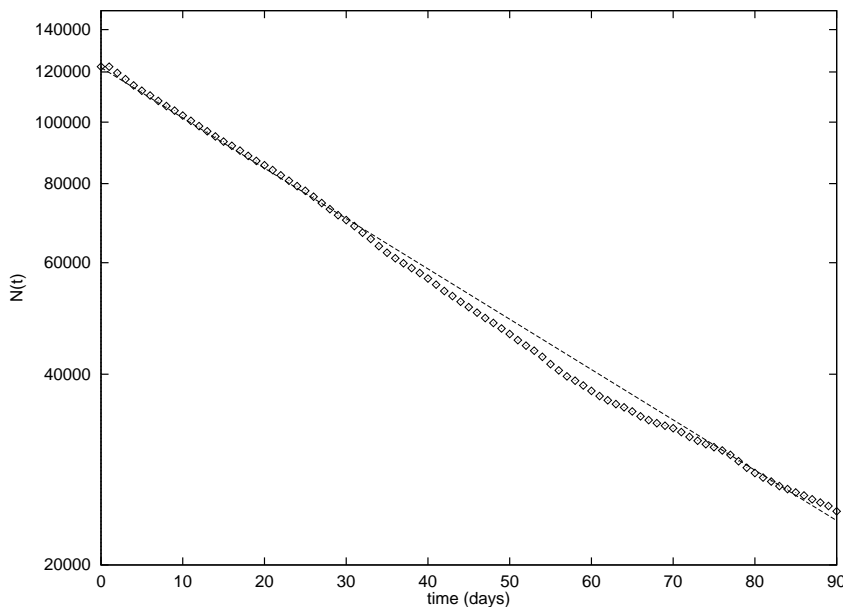

Fig. 4. The number of particles that did not leave the southern box in Fig. 1 after being deployed at the beginning of Winter in the first simulation year (symbols). The escape rate is obtained by an exponential fitting (dashed line).

5.2 North-South exchange

We focus here on transport between the northern and southern regions of the western Mediterranean (Fig. 1), by using the modified leaking method, or exchange method.

A particle started in the south is considered to be exchanged to the north when it first hits the northern box, and viceversa. Exchange during $\tau = 90$ days is nearly equivalent to a simple crossing of the 39N parallel. This is so because
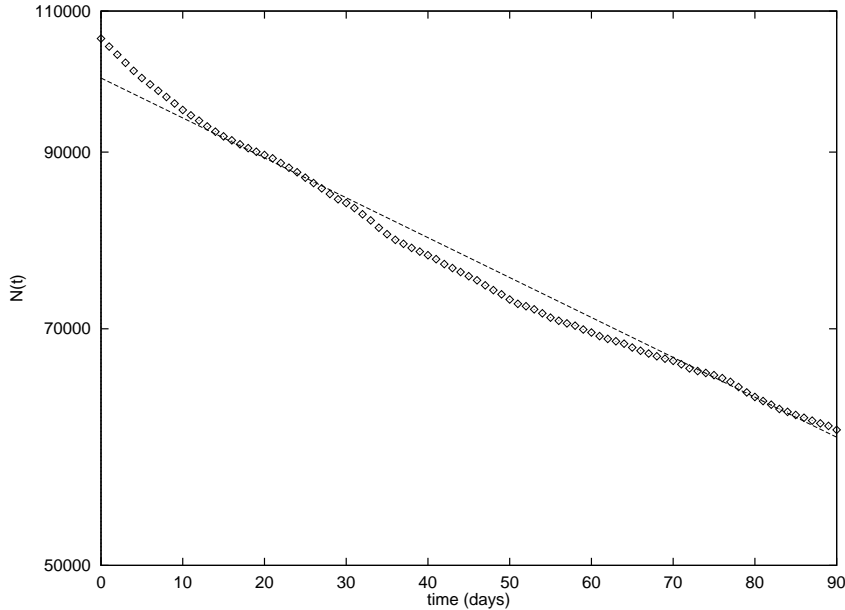
Fig. 5. The number of non-exchanged particles $N(t)$, i.e. the ones that did not exchange to the northern box a time t after starting from the southern one in Winter of the first simulation year (symbols). The dashed line is an exponential function decaying with the average rate $\bar{\kappa}$ defined in the text.

of the location of the boxes and of the coast, and because particles leaving the southern box towards the east will need a time longer than three-four months to reach the northern box moving along the Italian coast. Therefore, with the given geometry of the surroundings of the boxes, the exchange is comparable to a simple crossing, and the exchange rate equivalent to a crossing rate. Nevertheless, in the computations we use the criteria presented when explaining the exchange method.

As before, we initially fill-up the southern (northern) box with a large number of particles. $N(t_0) = 105791$ ($N(t_0) = 93675$) of them did not start in land and were followed until exchange to the other box occurred. Figure 5 shows the decay in the number of non-exchanged particles starting from the southern box in Winter of the first simulation year. It is clear that the decay now is not a simple exponential. The reason is that, as time advances, the particles are in average further and further away from the target region, so that the rate decreases in time. However, we can define an *average* exchange rate as $\bar{\kappa} = \tau^{-1} \ln\left(N(t_0)/N(t_f)\right)$, which characterizes the effective rate of exchange between the two regions during the considered integration time. For the example of Fig. 5 we find $\bar{\kappa} = 2.91 \cdot 10^{-3}$ days^{-1}. Note that, given that the inverse of this value (343.6 days) is much longer than the integration time ($\tau = 90$) we can not take it as a reliable average residence time. The value of $\bar{\kappa}$ however, when multiplied by the volume of water associated to the initial box, would give an estimation of the effective volume transport rate towards the second box during the integration time.

12

	N to S	(std)	S to N	(std)
Winter	$3.06 \cdot 10^{-3}$	$(2.75 \cdot 10^{-4})$	$6.59 \cdot 10^{-3}$	$(6.43 \cdot 10^{-4})$
Spring	$2.38 \cdot 10^{-3}$	$(1.39 \cdot 10^{-3})$	$5.89 \cdot 10^{-3}$	$(1.24 \cdot 10^{-3})$
Summer	$2.91 \cdot 10^{-3}$	$(6.91 \cdot 10^{-4})$	$6.11 \cdot 10^{-3}$	$(1.31 \cdot 10^{-3})$
Autumn	$3.03 \cdot 10^{-3}$	$(3.18 \cdot 10^{-4})$	$3.83 \cdot 10^{-3}$	$(5.96 \cdot 10^{-4})$
Yearly Average	$2.84 \cdot 10^{-3}$	$(3.16 \cdot 10^{-4})$	$5.6 \cdot 10^{-3}$	$(1.2 \cdot 10^{-3})$

Table 2
Seasonal exchange rates between the two boxes (in day^{-1}) averaged over the 4 years, and the associated standard deviation (std) characterizing variability among the 4 year s.

Table 2 summarizes the seasonal ($\tau = 90$) crossing rates $\overline{\kappa}$ among the two boxes, averaged over 4 years, with the corresponding standard deviations giving an indication on the interannual variability in the crossing rates.

We see that there is a seasonal variability of the crossing rates, being Winter the season in which more exchange occurs in both directions, and also the one recording the maximum imbalance between them. This imbalance is strong during all the seasons except Autumn, so that there is a net annual rate from south to north, implying that surface Atlantic waters from the Algerian subbasin are, on average, crossing the 39N line and mixing with saltier waters in the north. This northward surface transport must be compensated by a net southward transport of saltier (denser) water in deeper layers.

To get more insight into the transport locations, we investigate the initial and final positions of the particles released in each of the boxes. We plot in Fig. 6 the *exchange set* from south to north, i.e. the set of southern initial conditions which bring water to the northern box during the interval of time τ. The shape of the exchange set changes each season, according to the seasonal dependence of the exchanging or crossing rates. The exchange set is smallest in Autumn in correspondence to the smaller crossing rate in Table 2. The exchange set is denser close to the boundary between the regions, indicating an easier crossing towards the north for the particles starting there, but it extends deep into the interior of the southern box, forming filamental structures interleaved with the non-exchanged set. Eddy structures, specially their outer parts, are clearly involved in the northern transport.

The eastern part of the Algerian region tends to be excluded from the exchange set, specially in Autumn. Particles started there will be transported eastward
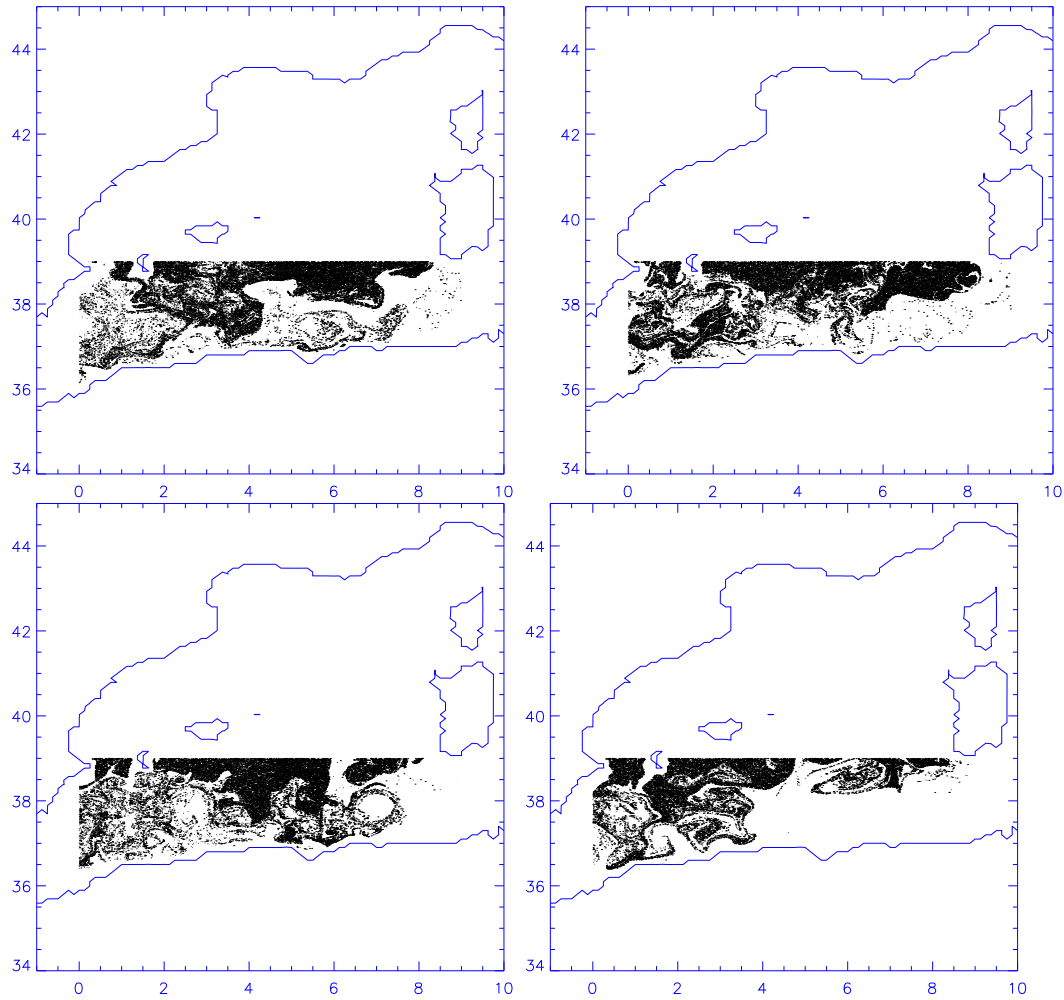
Fig. 6. Exchange sets towards the northern box starting in the south at different seasons (first simulation year): Upper left: Winter, upper right: Spring, lower left: Summer, lower right: Autumn.

by the Algerian current. This can be seen when plotting the final positions of the particles which did not exchange into the northern box. As the previous pictures, Fig. 7 shows these positions for particles started in the southern box in Winter. Non-exchanged particles followed the Algerian current along the African coast towards the East. Shortly before reaching the Channel of Sicily, the current splits into two parts: one going into the Tyrrhenian subbasin (reaching the northern box along this route would take more than the 90 days used in this computation), and the other one following the coastal current along the African coast into the eastern basin of the Mediterranean, where we can see that they also follow an alongslope cyclonic circulation. However, some particles are still in their initial southern box. They seem to be trapped in several vortexes close to the African coast.

Fig. 8 shows another sequence of the exchange sets, but this time towards the southern box for particles launched in the north. In comparison with the
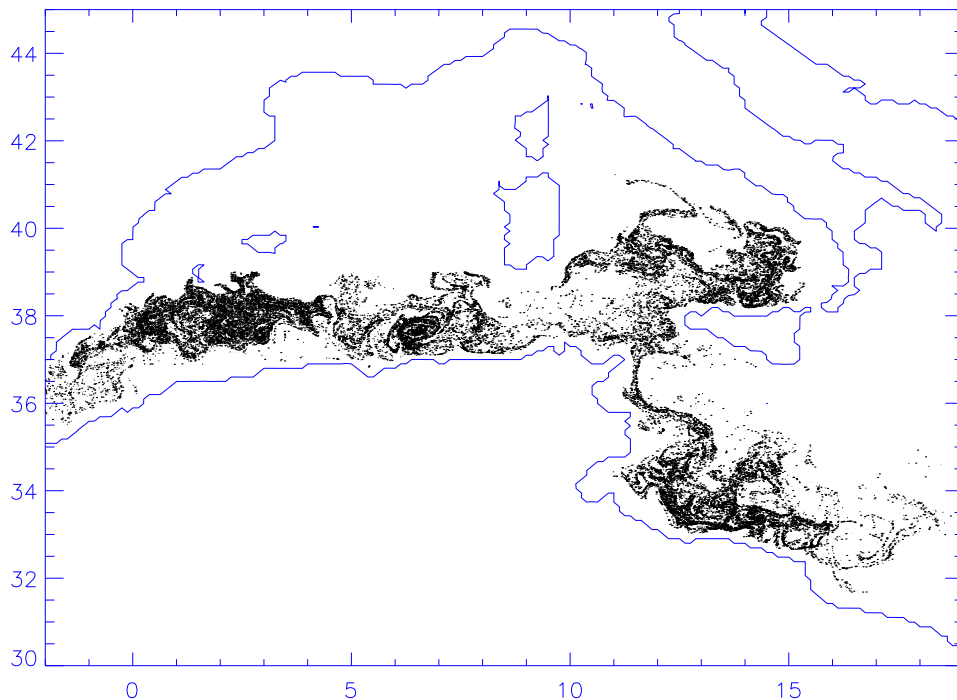
Fig. 7. Final positions (after $\tau = 90$ days) of particles launched in Winter (first simulation year) in the southern box which did not exchange to the North.

exchange sets in Fig. 6, here they are more restricted to the neighborhood of the crossing boundary, except for the presence of a coastal current along the Spanish coast (the so-called Northern Current), more visible in Autumn and less intense in the Summer. This reflects the fact that in the numerical simulation, the Northern Current transports some waters towards the Algerian subbasin through the Ibiza channel, but part of it is deflected to the north of the Balearic Islands (Fernández et al., 2004). In accordance with the smaller crossing set, the crossing rates shown in Table 2 are also smaller. At all seasons, the exchange set excludes a region starting north of the Mallorca channel (the channel between Ibiza and Mallorca islands) and extending northeast. This identifies the location of a strong current transporting particles in the northeast direction, which can be associated with the Balearic current (Pinot et al., 2002) .

To get additional indications of the mixing between different water masses, we plot in Fig. 9 final positions of particles which exchanged from the northern towards the southern box during the 90 days integration, starting in Winter. Many particles are tracing out the same structures as particles launched in the south: both are showing the routes of transport of the main circulation in the basin, partly going to the eastern basin of the Mediterranean. Thus mixing of water from both origins is occurring along these routes. There are however differences. For example there is some accumulation of particles southwest
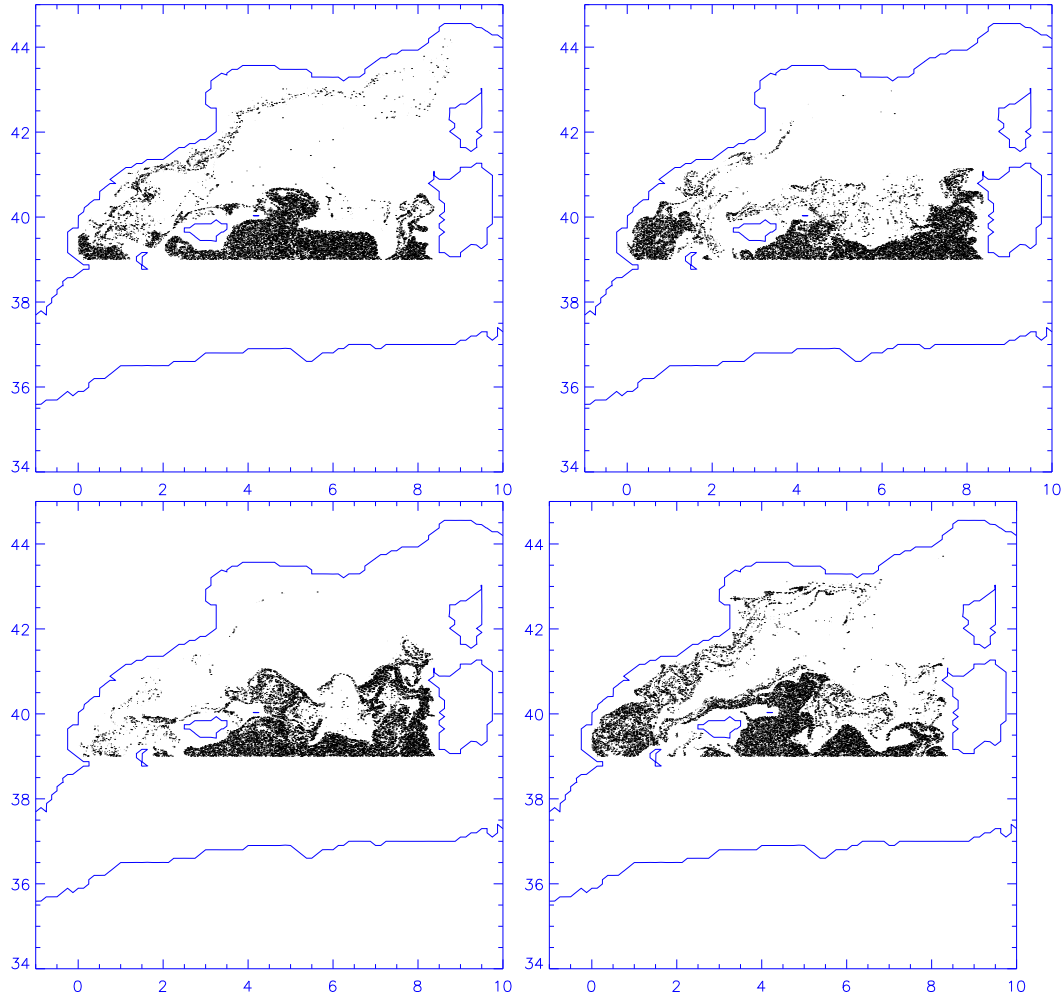
15

Fig. 8. Exchange sets towards the southern box starting in the north at different seasons (first simulation year): Upper left: Winter, upper right: Spring, lower left: Summer, lower right: Autumn.

of Sardinia island, indicating that many of the exchanged particles remain recirculating in that area. In addition, eddy structures are less evident here, in particular for the further reaching particles, than in Fig. 6. From this and other comparisons between Figs. 6, 7, 8 and 9, we can conclude that transport mediated by vortices is more important for the south-north direction than for the reverse, corresponding to the abundance and origin of these structures close in the Algerian subbasin (Millot, 1999; Salas et al., 2002).

5.3 The impact of additional diffusive processes

Our ocean model velocity fields, as any others obtained from models or data of finite resolution, lack structures below the horizontal grid size, which is 1/8 of degree (10-12 km) in our case. Computation of Lagrangian trajectories uses
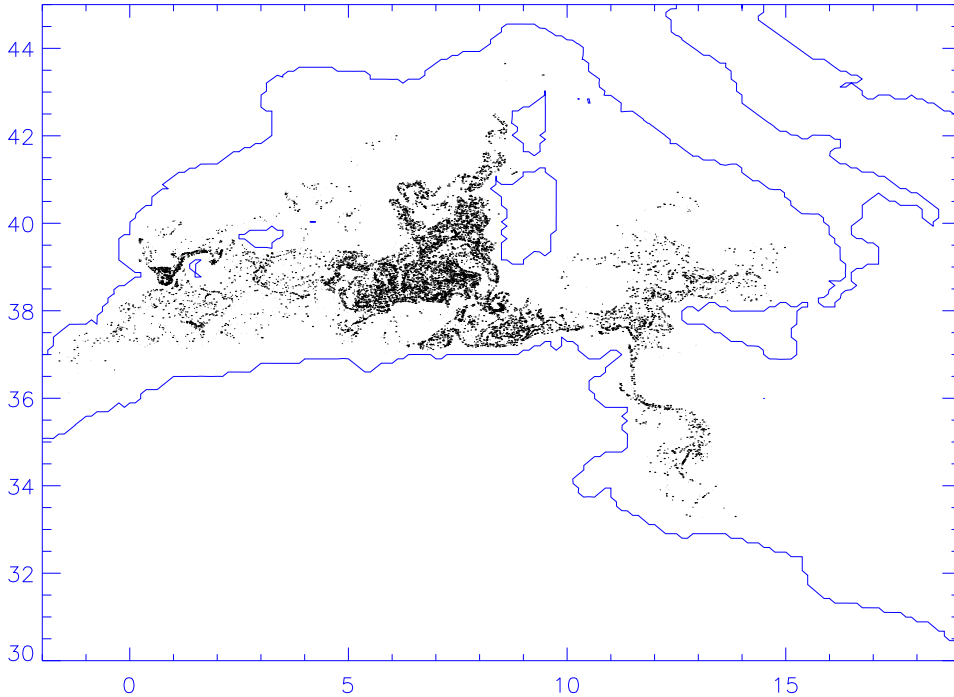
16

Fig. 9. Final positions (after $\tau = 90$ days) of particles launched in Winter (first simulation year) in the northern box which did exchange to the South.

spatial interpolation to follow the particles and thus Lagrangian geometrical features can be obtained that are smaller than this limit (see for example Fig. 3). Thus there is the question on how realistic are these small structures and how the different rates calculated here will change when including smaller scales in the numerical model. A convenient way to include unresolved scales in Lagrangian computations is to add to the velocity field experienced by the Lagrangian particle a fluctuating term representing small-scale turbulence (Griffa, 1996; Mariano et al., 2002): $\dot{\mathbf{x}}(t) = \mathbf{v}(\mathbf{x}(t), t) + \sqrt{2K}\Gamma(t)$. This gives additional diffusion to particle trajectories. Usually $\Gamma(t)$ is taken to be a Gaussian Markov process with a memory time that for Mediterranean modelling is of the order of some days (Buffoni et al., 1997; Falco et al., 2000). This kind of Markov process leads to a situation that is somehow in between the purely deterministic calculation using the model velocity field alone, and the larger stochasticity that is obtained when $\Gamma(t)$ is a memoryless white noise. Here, to explore the impact of irregular unresolved motions in the opposite extreme to the deterministic situation considered in the previous sections, we use for $\Gamma(t)$ a Gaussian white noise of zero mean and correlations $\langle \Gamma(t)\Gamma(t') \rangle = \delta(t - t')$. We take for its strength K the same value of the horizontal diffusivity K_h used in the model simulations $K_h = 10\ m^2 s^{-1}$, which in turn was the same value, as discussed in Sect. 3, estimated by Okubo (1971), as the effective diffusivity at the scale of the model grid. After integrations sufficiently longer

17

	N to S	(std)	S to N	(std)
Winter	$3.11 \cdot 10^{-3}$	$(2.74 \cdot 10^{-4})$	$6.82 \cdot 10^{-3}$	$(6.59 \cdot 10^{-4})$
Spring	$2.45 \cdot 10^{-3}$	$(2.61 \cdot 10^{-4})$	$6.19 \cdot 10^{-3}$	$(1.23 \cdot 10^{-3})$
Summer	$3.04 \cdot 10^{-3}$	$(6.81 \cdot 10^{-4})$	$6.38 \cdot 10^{-3}$	$(1.4 \cdot 10^{-3})$
Autumn	$2.77 \cdot 10^{-3}$	$(7.22 \cdot 10^{-4})$	$4.07 \cdot 10^{-3}$	$(6.53 \cdot 10^{-4})$
Yearly Average	$2.84 \cdot 10^{-3}$	$(2.99 \cdot 10^{-4})$	$5.87 \cdot 10^{-3}$	$(1.2 \cdot 10^{-3})$

Table 3
Exchange rates (in day^{-1}, averaged over the 4 simulation years) between the two boxes at different seasons, and the associated standard deviation (std), in the presence of Lagrangian diffusion. To be compared with table 2.

than the memory time, no significant differences are expected between using this uncorrelated motion or the more realistic Markov process (Griffa, 1996; Buffoni et al., 1997; Falco et al., 2000; Mariano et al., 2002) for the Lagrangian diffusion.

Table 3 shows the recalculated exchange rates, to be compared with table 2. We see that the impact of adding Lagrangian diffusion is not strong. In most of the cases the effect is the intuitively expected slight acceleration of the rates, although there is a case in which diffusion slows down the exchange process. This will occur when diffusion kicks-off particles from the fine structures in the main transport routes.

In Fig. 10 we show examples of the spatial Lagrangian structures obtained in the presence of diffusion. We plot the exchange set towards the northern box starting in Winter in the southern box (to be compared with the diffusionless first panel in Fig. 6) and the final positions of particles started in the southern box and not exchanged with the northern one (to be compared with the diffusionless Fig. 7). We see that the main characteristics of the deterministic evolution are retained. However, the smallest structures, including the finest filaments, are smoothed out, and this will occur in all the types of Lagrangian structures visualized. This does not mean that the sensitive dependence of the fate of particles to small displacements is lost. At the contrary, since both exchanged and non-exchanged sets are smoothed-out, they become still more intimately interleaved (mixed) at the smallest scales than in the absence of diffusion.

We remark that a slight smearing of the smallest spatial structures was also found in some simulations (without Lagrangian diffusion) in which an hourly-
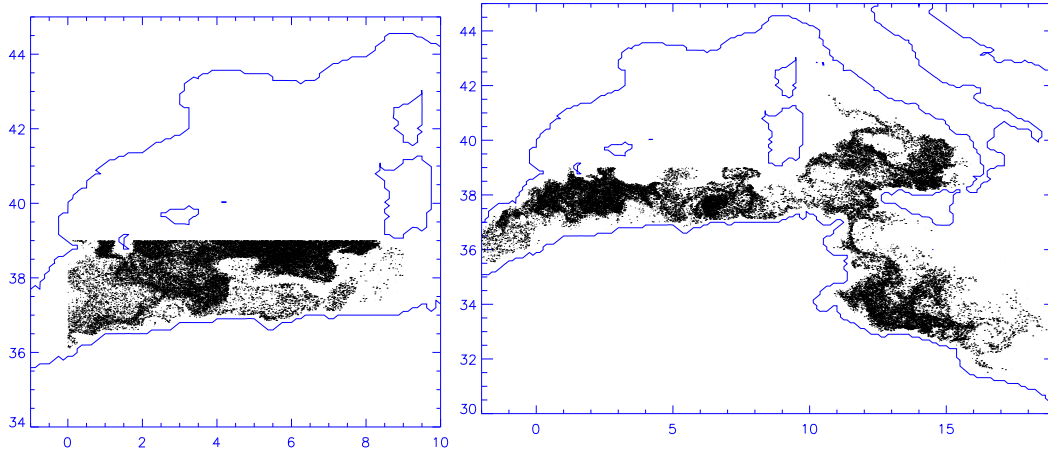
Fig. 10. Geometric structures in the presence of Lagrangian diffusion. Left: Exchange set towards the north of particles started in Winter in the southern box. To be compared with the diffusionless case in the first panel of Fig. 6. Right: Final positions (after $\tau = 90$ days) of particles launched in Winter in the southern box which did not exchange to the north. To be compared with the diffusionless case of Fig.7.

sampled velocity field was used instead of the daily-sampled fields used through this paper. This may indicate that the Lagrangian diffusion strategy could be useful not only to represent unresolved spatial scales, but also high frequency temporal variability (e.g. inertial oscillations).

6   Conclusion

In this Paper we have analyzed and quantified, from surface velocity fields provided by a numerical model, several transport processes involving different water masses in the Western Mediterranean. We have characterized their seasonal variability by calculating seasonal exchange rates and residence times. The geometry of the exchange sets and the transport locations has also been investigated.

Residence times smaller than a season have been found inside a southern region representing the Algerian subbasin. Eddies and other complex structures are involved in the exit process from this region, being the eastern part of the region the one with fastest escape.

Exchange of Atlantic waters towards the northern basin occurs at a higher rate, in the surface layer, than the reverse exchange. In agreement with Millot (1999), eddies in the Algerian subbasin play an important role in this transport, that is very seasonal and presents also a component of interannual variability. We expect the transport of saltier water towards the south to be

19

more intense in deeper layers, but at surface it involves only the areas close to the boundary between the regions, and the Northern Current. Eddy structures are not so prominent for this transport.

Small-scale turbulent process, modelled here as Lagrangian diffusion, modify the exchange rates in some small amount, but does not change the qualitative picture. Furthermore, the main structures and locations of transport remain, although they become smeared out (implying stronger mixing) at small scales.

The time scales obtained using the present Lagrangian approach based on a climatological numerical simulation of the Mediterranean are only a first approximation to the dynamics of the real Mediterranean. A numerical simulation using more accurate synoptic atmospheric forcing, including water mass formation, and a 3D study would give more realistic results. However, we showed that the present configuration of the model gives enough complexity to define filamental structures and transport locations between regions in the Mediterranean, as well as to define the complex transport by mesoscale eddies.

To conclude, we have shown that tools such as the leaking and the exchange methods are able to identify and characterize dynamical structures in aperiodic realistic flows, such as our numerically generated Mediterranean circulation. The methods allow to visualize the exchange sets and transport routes in a fast and efficient way. Understanding and good modelling of these structures is important to improve forecasting in practical situations: active or passive tracers released on places belonging to the exchange sets, such as for example an oil spill, will spread towards the target region.

References

M. Astraldi, S. Balopoulos, J. Candela, J. Font., M. Gacic, G.P. Gasparini, B. Manca, A. Theocharis, J. Tintoré, 1999. The role of straits and channels in understanding the characteristics of Mediterranean circulation. Progr. Oceanogr. 44, 65-108.

G. Buffoni, P. Falco, A. Griffa, E. Zambianchi, 1997. Dispersion processes and residence times in a semi-enclosed basin with recirculating gyres: An application to the Tyrhenian Sea. J. Geophys. Res. 102 (C8), 18699-18713.

C. Coulliette, S. Wiggins, 2001. Intergyre transport in a wind-driven, quasi-geostrophic double gyre: An application of lobe dynamics. Nonlinear Proc. Geophys. 8, 69-94.

D.E. Dietrich, 1997. Application of a modified 'a' grid ocean model having reduced numerical dispersion to the Gulf of Mexico circulation. Dyn. of Atm. and Oceans 27, 201-217.

D.E. Dietrich, R.L. Haney, V.Fernández, S. A. Josey, J. Tintoré, 2004. Air-Sea fluxes based on observed annual cycle surface climatology and ocean model internal dynamics: a non-damping zero-phase-lag approach applied to the Mediterranean Sea. J. Mar. Syst., 52, 145-165.

F. d'Ovidio, V. Fernandez, E. Hernández-García and C. Lopez, 2004. Mixing structures in the Mediterranean Sea from Finite-Size Lyapunov Exponents. Geophys. Res. Lett., 31, L17203, doi:10.1029/2004GL020328.

P. Falco, A. Griffa, P.M. Poulain, E. Zambianchi, 2000. Transport properties in the Adriatic Sea as deduced from drifter data. J. Phys. Oceanogr. 30, 2055-2071.

V. Fernández, D.E. Dietrich, R.L. Haney, J. Tintoré, 2004. Mesoscale, seasonal and interannual variability in the Mediterranean Sea using a numerical ocean model. Progr. Oceanogr., *in press.*

A. Griffa, 1996. Applications of stochastic particle models to oceanographic problems. in *Stochastic Modelling in Physical Oceanography*, R.J. Adler, P. Muller, and B.L. Rozovskii, Eds. Birkhauser, Boston. pp. 114-140.

G. Haller, A.C. Poje, 1998. Finite time transport in aperiodic flows. Physica D 119, 352-380.

B. Joseph, B. Legras, 2002. Relation between kinematic boundaries, stirring, and barriers for the Antarctic Polar vortex. J. Atm. Sci. 59, 1198-1212.

C. Jung, T. Tél and E. Ziemniak, 1993. Application of scattering chaos to particle transport in a hydrodynamical flow. Chaos 3, 555-568.

L. Kuznetsov, M. Toner, A.D. Kirwan Jr., C.K.R.T. Jones, L.H. Kantha, J. Choi, 2002. The loop current and adjacent rings delineate d by Lagrangian analysis of the new-surface flow. J. Marine Res. 60, 405-429.

G. Lacorata, E. Aurell, A. Vulpiani, 2001. Drifter dispersion in the Adriatic Sea: Lagrangian data and chaotic model. Annales Geophysicae 19, 121-129.

A.J. Mariano, A. Griffa, T.M. Özgökmen, E. Zambianchi, Lagrangian analysis and predictability of coastal and ocean dynamics 2000, 2002. J. Atm. Ocean. Tech. 19, 1114-1125.

C. Millot, 1987. Circulation in the Western Mediterranean. Oceanol. Acta 10 (2), 143-149.

C. Millot, 1991. Mesoscale and seasonal variabilities of the circulation in the Western Mediterranean. Dyn. Atm. Oceans 15, 179-214.

C. Millot, 1999. Circulation in the Western Mediterranean Sea. J. Mar. Syst., 20, 423-442.

A. Okubo, 1971. Oceanic diffusion diagrams. Deep-Sea Research 18, 789-802.

J.M. Ottino, 1989. The kinematics of mixing: stretching, chaos and transport. Cambridge University Press, Cambridge, UK.

R.C. Pacanowski, S.G.H. Philander, 1981. Parameterization of vertical mixing in numerical models of tropical oceans. J. Phys. Oceanogr. 11, 1443-1451.

A. Pascual, B. B. Nardelli, G. Larnicol, M. Emelianov, D. Gomis, 2002. A case of an intense anticyclonic eddy in the Balearic Sea (Western Mediterranean). J. Geophys. Res., 107 (C11), 3183, doi:10.1029/2001JC000913.

J.M. Pinot, J.L. López-Jurado, M. Riera, 2002. The CANALES experiment (1996-1998). Interannual, seasonal, and mesoscale variability of the circulation in the Balearic channels. Progr. Oceanogr. 55, 335-370.

J. Salas, C. Millot, J. Font, E. García-Ladona, 2002. Analysis of mesoscale phenomena in the Algerian Basin observed with drifting buoys and infrared images. Deep-Sea Res., 49, 2, 245-266.

J. Schneider, T.Tél, 2003. Extracting flow structures out of tracer data. Ocean Dynamics 53, 64-72.

J. Schneider, T. Tél, Z. Neufeld, 2002. Dynamics of leaking Hamiltonian systems. Phys. Rev. E 66, 066218.

E. Ott and T. Tél, 1993. Chaotic scattering: an introduction, Chaos 3, 417-426.

I. Taupier-Letage and C. Millot, 1986. Surface circulation in the Algerian Basin during 1984. Oceanol. Acta 9 (2), 119-131.

I. Tuval, J. Schneider, O. Piro, T. Tél, 2004. Opening up fractal structures of three dimensional flows via leaking. Europhys. Lett. 65, 633-639.

S. Wiggins, 1992. Chaotic Transport in Dynamical Systems. Springer Verlag, New York.